

# TWO-AXIS CAPACITIVE MEMS-BASED ACCELEROMETER FOR ORIENTATION SENSING IN THE X- AND Z-AXES

B. Bernier

Department of Electrical and Computer Engineering  
The George Washington University, Washington, DC

## ABSTRACT

This paper discusses a two-axis capacitive MEMS accelerometer used for orientation sensing in both the x and z-axes. The accelerometer uses interdigitated comb fingers attached to a large proof mass in the x-axis and a single varying capacitance in the z-axis to measure accelerations up to  $\pm 2g$  ( $19.6m/s^2$ ). The complete design is presented in detail as well as a model that was created in CoventorWare and analyzed using its FEM simulator. Both analytical and simulated results are presented in detail.

## INTRODUCTION

### Background

Applications for accelerometers are widespread from handheld consumer electronic devices to airbag safety systems in automobiles. Spinning disk hard drives use accelerometers to detect zero-g conditions, likely meaning they have been dropped, and smartphones use accelerometers to change the orientation of the screen.

There are multiple methods for producing MEMS-based accelerometers including those using piezoresistive materials [1]; micro-cantilevers [2]; and the method chosen here, capacitive comb fingers [3].

One of the primary examples of a capacitive accelerometer using comb fingers is Analog Device's ADXL50, which is capable of measuring  $\pm 50g$  [4]. Figure 1 shows the actual ADXL50 structure under the microscope, depicting the beam and proof mass structure as well as the fixed comb fingers between them.

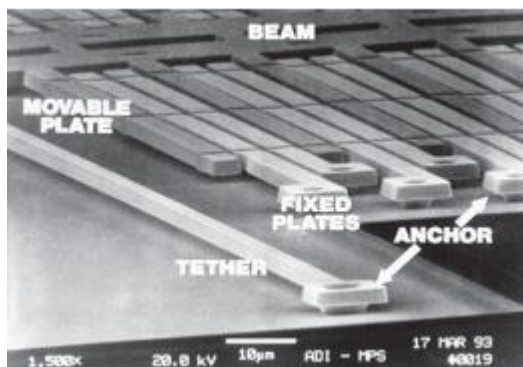


Figure 1: ADXL50 structure under scanning electron microscope (SEM). [5]

### Motivation

The motivation behind the analysis of a capacitive accelerometer described in this paper stems from a device I made for my senior design project that protects the visually impaired from collisions. The system consists of a headset and cane attachment, both capable of detecting obstacles in

the user's path and reporting that information back to the user. Accelerometers are used in both devices to determine the orientation of the user's cane and head. This provides the ability to notify a user when their cane is improperly oriented and to ignore irrelevant data. The system currently makes use of Freescale Semiconductor's MMA7361L [6] three-axis low-g capacitive micromachined accelerometer. This particular accelerometer has a sensing range of  $\pm 1.5g$ . The sensing range of  $\pm 2g$  specified in this paper allows for easy orientation sensing (static effect of gravity on a given axis) as well as allowing for an additional 1g of acceleration in either direction.

## STRUCTURAL DESIGN

### Fabrication Process

The following eleven step process flow shows the entire fabrication process from the bare silicon wafer to the actual accelerometer. The final few images depict the cross sections of just the fixed fingers of the accelerometer.

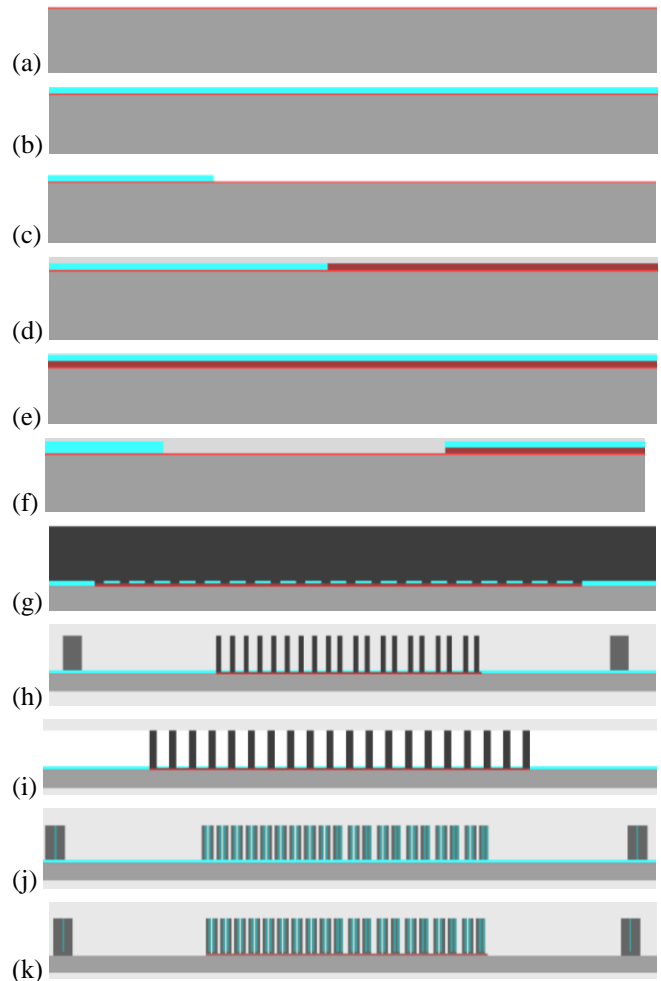


Table 1: Fabrication process details.

Step	Details
a	LPCVD Silicon Nitride Deposition
b	Sacrificial Polyimide Deposition
c	Polyimide Patterning: RIE Plasma Etch
d	LPCVD Polysilicon Deposition
e	Second Sacrificial Layer
f	Second Polyimide Patterning
g	Aluminum Sputter Deposition
h	Aluminum Patterning: RIE Plasma Etch
i	Aluminum Deposition
j	Aluminum Patterning: RIE Plasma Etch
k	Release of Sacrificial Polyimide Material

The passivation layer of silicon nitride in step (a) serves to isolate the structure from the substrate. The sacrificial layer serves to lift the entire accelerometer up off of the substrate  $1\mu\text{m}$  to allow its proof mass to freely move. The remainder of the steps pertain to patterning the wafer properly to obtain the necessary elements for the design including the anchors, proof mass, and comb fingers. Step (d) includes depositing a layer of polysilicon underneath the proof mass that acts as an electrode and the lower plate of a large parallel plate capacitor with the proof mass.

Aluminum was chosen to be the primary material comprising the proof mass and tethers because it has a relatively low Young's Modulus (77 GPa) while maintaining an average density when compared to other process material options. The smaller Young's Modulus allows for more sensitive acceleration detection in the low-g range. Note that on the left and right of the proof mass in Figure 2 are two bumpers that prevent the mass from swaying too far in the x-axis.

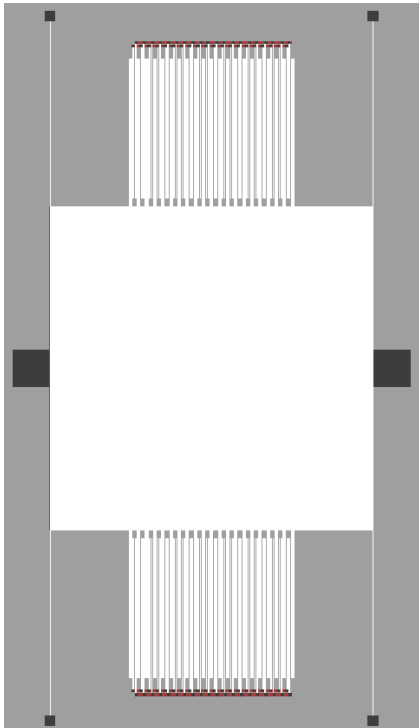


Figure 2: Top view of complete accelerometer structure.

## ANALYTICAL DESIGN

### Overview

The design of this accelerometer started with designing the overall comb and proof mass structure that allows acceleration measurement in the x-axis. This portion of the design was largely derived from Figure 3 below [7].

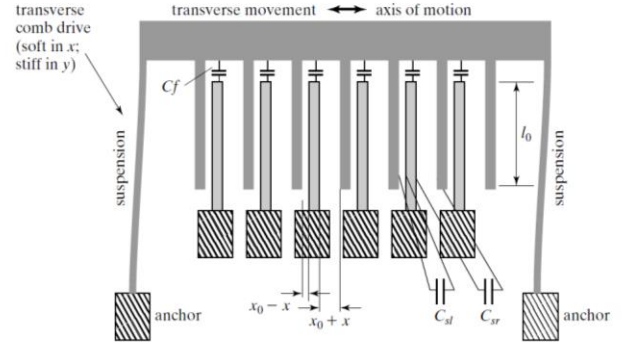


Figure 3: Schematic of transverse comb drive.

To start, a few of the variables were chosen as fixed values so that the remainder of the parameters could be calculated. The model of the transverse comb drive was doubled, so that the total number of beams supporting the proof mass was 4, while allowing a greater capacitance to be measured on the comb fingers by adding 20 fixed sets of fingers on each side of the proof mass. The four fixed-guided beams were chosen to be  $250\mu\text{m}$  long,  $1.5\mu\text{m}$  thick, and  $20\mu\text{m}$  wide. Because the beams deflect along the x-axis, the thickness is defined as the x-dimension while its width is along the z-axis.

The beams attached to the proof mass are  $200\mu\text{m}$  long,  $5\mu\text{m}$  wide, and  $20\mu\text{m}$  thick. Each fixed comb finger is separated into a left and right finger, each  $2\mu\text{m}$  wide,  $20\mu\text{m}$  thick, separated from the beams by  $x_0 = 0.5\mu\text{m}$ . The overlap length  $l_0$  was also chosen to be  $190\mu\text{m}$ .

### Mechanical Design

Defining the mechanical behavior of the designed structure is important to characterizing its overall response to acceleration. The spring constant for a single fixed-guided beam is given to be [7]

$$k = \frac{12EI}{L^3} \quad (1)$$

where

$$I = \frac{wt^3}{12} \quad (2)$$

E in this equation refers to the Young's Modulus for the material being used, while w, t, and L are the width, thickness, and length of an individual fixed-guided beam, respectively. Because there are four total beams supporting the proof mass, the overall spring constant is simply four times the individual spring constant.

$$k_{tot} = 4 * \frac{12EI}{L^3} \quad (3)$$

By Hooke's Law:

$$F = k_{tot}x \quad (4)$$

and the overall displacement in the x-axis can be defined as

$$\Delta x = \frac{FL^3}{48EI} = \frac{maL^3}{4Ewt^3} \quad (5)$$

By setting x equal to the maximum displacement when a is equal to 2g, we can solve for the remainder of the necessary variables. At first, the maximum displacement was assumed to be the full initial gap, 0.5 $\mu$ m; however, if this were the case, the capacitance would not be linear. Instead, the maximum displacement was taken to be 0.16 $\mu$ m after some initial testing which showed the capacitance to change fairly linearly up to that point.

Solving for the acceleration provides a direct linear relationship between the displacement x and acceleration a.

$$a = \frac{4Ewt^3x}{mL^3} \quad (6)$$

Since the accelerometer is specified to be within the  $\pm 2g$  range, that knowledge can be used to determine the necessary proof mass, if all other values are assumed ahead of time.

$$m = \frac{4Ewt^3x}{aL^3} \quad (7)$$

From this equation, it is determined that m must be 1.086x10<sup>-8</sup>kg. From here, assuming the proof mass to be square with a side of length s, the dimensions of the proof mass can be determined from Equation 8, where t is the thickness of the proof mass,  $\rho$  is the density of the material, in this case aluminum, 2.3x10<sup>-15</sup>kg/m<sup>3</sup>, n is the number of beam fingers attached to the proof mass, and w and l are the width and length of each comb finger.

$$s = \sqrt{\frac{m}{\rho t} - nwL} \quad (8)$$

Finally, the resonant frequency of the accelerometer can be calculated for the first two modes with the following equation, bearing in mind that the spring constant is different in the x- and z-axes. In the z-axis, w and t from Equation 2 are reversed, which holds for all calculations.

$$f = \frac{1}{2\pi} \sqrt{\frac{k_{tot}}{m}} \quad (9)$$

This provides the necessary information to determine the mechanical bandwidth of the accelerometer. Because Equation 5 only holds true at frequencies much lower than the resonant frequency of the device, the bandwidth is assumed to be roughly 10% of the resonant frequency [8].

## Electrical Design

The electrical behavior of this accelerometer is dependent on the capacitances between the comb fingers in the x-axis and between the proof mass and electrode in the z-axis. Equation 10 shows the capacitance on each fixed finger and the moving proof mass

$$C = \frac{\epsilon_0 l_0 t}{x} \quad (10)$$

The total measured capacitance for the x-axis with 40 fixed fingers can be calculated as

$$C_{tot} = 40 \left( \frac{\epsilon_0 l_0 t}{x} + C_f \right) \quad (11)$$

In the z-axis, the capacitance can similarly be found as in Equation 10, with the area of the proof mass being the area of the capacitor.

$$C = \epsilon_0 \frac{S^2}{z} \quad (12)$$

Taking the partial derivative of the total capacitance with respect to the acceleration gives the relative change of capacitance with respect to acceleration in the x-axis.

$$\frac{\partial C_{tot}}{\partial a} = \frac{10\epsilon_0 l_0 L^3 m}{Et^2 w \left( x_0 - \left( \frac{L^3 a m}{4Et^3 w} \right)^2 \right)} \quad (13)$$

## NUMERICAL MODEL

### Modal Simulation

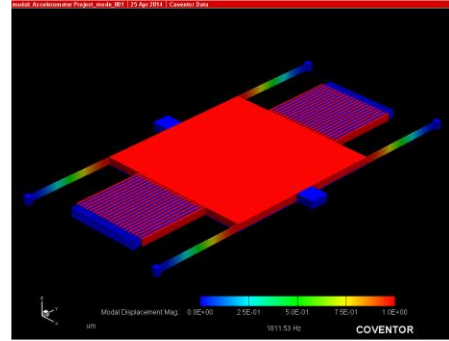


Figure 4: Simulated x-axis resonant frequency.

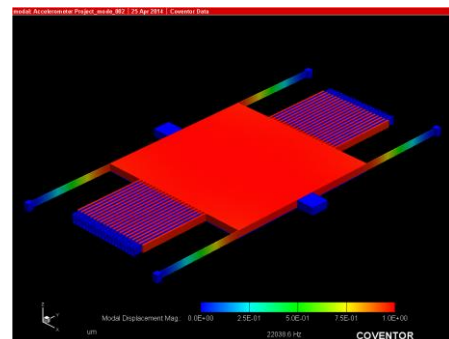


Figure 5: Simulated z-axis resonant frequency.

### Displacement vs. Acceleration

The following graphs compare the calculated results from Equation 5 with the simulated results from CoventorWare.

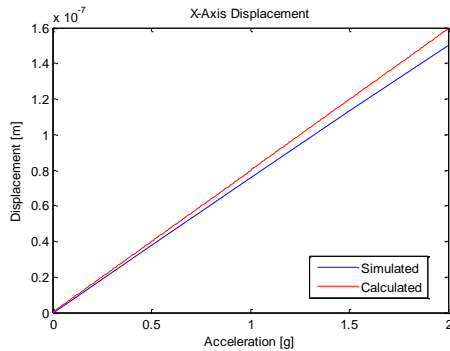


Figure 6: X-axis displacement vs. acceleration.

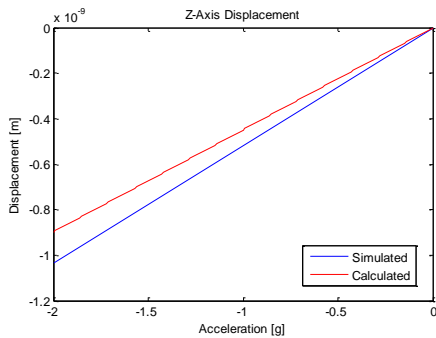


Figure 7: Z-axis displacement vs. acceleration.

### Capacitance vs. Acceleration

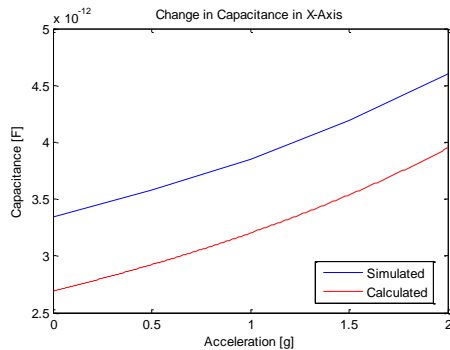


Figure 8: X-axis capacitance change vs. acceleration.

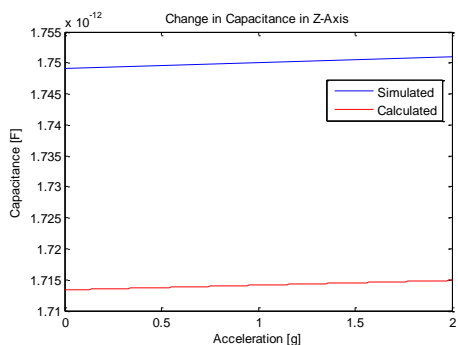


Figure 9: Z-axis capacitance change vs. acceleration.

The capacitance changes at roughly the same rate for both simulated and calculated results. The difference and shift in the simulated results is that it takes all of the fringe capacitances into account as well, which were not accounted for in the calculations here.

### Results

Table 2: Various calculated and simulated values showing low percent error, verifying the analytical design.

Value	Calculated	Simulated	Percent Error
mass [kg]	1.088e-8	1.085e-8	0.28%
$f_1$ [kHz]	1.7635	1.8115	2.65%
$f_2$ [kHz]	23.4633	22.0386	6.46%
$\Delta x @ 2g$ [ $\mu\text{m}$ ]	0.1596	0.1505	4.29%
$\Delta z @ 2g$ [nm]	0.8980	1.0329	13.06%
$C_x @ 0g$ [pF]	2.6918	3.2067	16.06%
$C_z @ 0g$ [pF]	1.7134	1.7847	4.00%

Table 3: Capacitive sensitivity of each axis.

X-axis	Z-axis
0.633pF/g	0.9fF/g

Table 4: Z-axis effect on x-axis accuracy

Z-axis Capacitance at 0g	X-axis Capacitance with 2g in Z-axis	Percent Error
3.2067pF	3.2100pF	0.10%

Table 5: X-axis effect on z-axis accuracy

Z-axis Capacitance at 0g	Z-axis Capacitance with 2g in X-axis	Percent Error
1.750531pF	1.750511pF	~0.00%

### REFERENCES

- [1] J. Lynch, A. Partridge, K. Law, T. Kenny, A. Kiremidjian, E. Carryer. "Design of Piezoresistive MEMS-Based Accelerometer for Integration with Wireless Sensing Unit for Structural Monitoring", in *ASCE Journal of Aerospace Engineering*, July 2003, pp. 108-114.
- [2] O. Sidek, M. Miskam, H. Khaleed, M. Alias, S. Mohd. "Optimal Design of Capacitive Micro Cantilever Beam Accelerometer", *Modern Applied Science*, Sept. 2009, pp. 16-28.
- [3] K. Sharma, I. Macwan, L. Zhang, L. Hmurcik, X. Xiong. "Design Optimization of MEMS Comb Accelerometer", University of Bridgeport, pp. 1-10.
- [4] ADXL50 Datasheet. Monolithic Accelerometer With Signal Conditioning. Analog Devices.
- [5] R. O'Reilly, A. Khenkin, K. Harney. "Sonic Nirvana: Using MEMS Accelerometers as Acoustic Pickups in Musical Instruments", *Analogue Dialogue*, Feb. 2009, pp. 1-4.
- [6] MMA7361L Technical Datasheet.  $\pm 1.5g$ ,  $\pm 6g$  Three Axis Low-g Micromachined Accelerometer. Freescale Semiconductor.
- [7] Liu, Chang. Foundations of MEMS. 2<sup>nd</sup> ed. Prentice Hall: Upper Saddle River, NJ, pp. 161-164.
- [8] S. Tseng, M. Lu, P. Wu, Y. Teng, H. Tsai, Y. Juang. "Implementation of a monolithic capacitive accelerometer in a wafer-level 0.18 $\mu\text{m}$  CMOS MEMS process", *Journal of Micromechanics and Microengineering*, April 2012, p. 6.